scientific reports

OPEN

A compact dual-band reconfigurable antenna with metamaterial for IoT applications

Abdullah Hasan Ali[1✉], Jamal Mohammed Rasool[2], Ali Kadhum Abd[2], Md. Shabiul Islam[3,4✉], Mohamed Ouda[5], Mohamad A. Alawad[6] & Mohammad Tariqul Islam[7✉]

This study presents a compact antenna designed for Internet of Things (IoT) applications, utilizing advanced wireless communication technologies. The antenna is designed to operate at dual frequencies (2.4 GHz and 6.04 GHz) with 12 multipath T-structured metamaterials. In Mode 1 (D1 OFF), the antenna operates at 2.4 GHz with a bandwidth of 80 MHz (2.36–2.44 GHz). In Mode 2 (D1 ON), it functions at 6.04 GHz with a bandwidth of 300 MHz (5.9–6.2 GHz). The design employs a commercially available FR-4 substrate with a relative permittivity of 4.3 and a loss tangent of 0.025, all within a compact size of $(0.16\lambda_0 \times 0.12\lambda_0 \times 0.0112\lambda_0)$. The antenna radiator integrates a single PIN diode (SMP1340-079LF) along with a complete biasing circuit to achieve reconfigurability. The proposed design overcomes the conventional limitations by integrating T-structured metamaterials to achieve dual-band operation in a compact size. This antenna is ideal for wireless communication applications due to its manufacturability, enhanced gain, and low return loss. It is well suited for widely used frequency ranges, including Wi-Fi and Bluetooth. The results demonstrate that a miniaturized antenna with excellent efficiency has achieved, making it a promising solution for next-generation IoT devices.

Keywords Dual-band, Internet of Things, Metamaterial, Positive intrinsic negative diode, Reconfigurable, Unit cell

The exponential growth of wireless communication technologies has profoundly transformed modern life, enabling real-time connectivity between people, devices, and systems across vast distances. One of the most significant technological trends of the past decade is the emergence and rapid expansion of the Internet of Things (IoT), a paradigm that envisions the interconnection of billions of smart devices capable of sensing, communicating, and processing data autonomously. These devices are expected to operate seamlessly within complex and heterogeneous networks, sharing information efficiently while consuming minimal power and occupying limited physical space[1,2].

This growing demand for ubiquitous, intelligent, and low-power connectivity has imposed new requirements on the design of wireless communication components, particularly antennas. As the core element responsible for transmitting and receiving electromagnetic signals, the antenna must meet several critical criteria in IoT systems: compactness, frequency flexibility, low energy consumption, and robust electromagnetic performance in dense environments[3,4]. In portable electronic devices including smartphones, tablets, smartwatches, GPS trackers, and medical wearables, the space allocated for the antenna is increasingly constrained. Nevertheless, the antenna must still maintain high performance across multiple frequency bands and wireless protocols such as Wi-Fi, Bluetooth, Zigbee, and Lora WAN[5].

Conventional antenna technologies often fall short when deployed in such demanding scenarios, as they typically require trade-offs between size, bandwidth, gain, and efficiency. In addition, the fixed-frequency operation of many legacy antennas limits their ability to adapt to dynamic wireless environments where multi-standard operation and interference mitigation are essential. IoT systems further exacerbate these challenges by

[1]College of Education for Pure Sciences, University of Diyala, Baquba, Iraq. [2]Department of Communication Engineering, University of Technology, Baghdad, Iraq. [3]Centre for Advanced Devices and Systems, Centre of Excellence for Robotics and Sensing Technologies, Multimedia University, Persiaran Multimedia, 63100 Cyberjaya, Selangor, Malaysia. [4]Faculty of Artificial Intelligence and Engineering, Multimedia University, Persiaran Multimedia, 63100 Cyberjaya, Selangor, Malaysia. [5]College of Engineering and Technology, University of Doha for Science and Technology, Doha, Qatar. [6]Department of Electrical Engineering, College of Engineering, Imam Mohammad Ibn Saud Islamic University (IMSIU), Riyadh, Saudi Arabia. [7]Department of Electrical, Electronic and Systems Engineering, University Kebangsaan (UKM), Bangi, Malaysia. ✉email: abdullah.hasan.ali@uodiyala.edu.iq; shabiul.islam@mmu.edu.my; tariqul@ukm.edu.my

requiring support for diverse device densities, adaptive power control, and coexistence within shared spectrum environments[6,7].

In response to these limitations, metamaterials and metasurfaces have emerged as promising solutions in the field of antenna engineering. Metamaterials are artificially structured materials designed to exhibit unconventional electromagnetic properties such as negative permittivity and/or permeability, which do not exist in naturally occurring substances[8]. These unique characteristics enable unprecedented control over wave propagation, radiation direction, and surface current distribution, opening the door to highly efficient and miniaturized antenna designs suitable for integration into IoT-enabled devices[9,10].

Furthermore, the advent of Frequency Reconfigurable Antennas (FRAs) has provided a practical pathway to address the dynamic requirements of modern communication systems. By integrating reconfigurable elements such as PIN diodes, varactor diodes, Micro-Electro-Mechanical Systems) MEMS (switches, or digital tuning components, FRAs allow antennas to switch between frequency bands, alter polarization, or modify radiation patterns in real-time based on network conditions or device requirements[11,12]. This capability is particularly valuable in IoT networks, where the operating environment may change rapidly, and the need for adaptive performance is paramount.

In this study, we propose an innovative antenna structure that combines the advantages of metamaterials and reconfigurability to meet the stringent demands of next-generation IoT systems. The proposed design incorporates embedded metasurfaces, multi-path configurations, and tunable components to achieve compact size, high radiation efficiency, and dynamic frequency agility. The antenna is optimized to operate in frequency bands relevant to IoT applications, including 2.4 GHz, 5 GHz, and emerging 6 GHz ranges, ensuring compatibility with a wide range of low-power communication protocols[13,14].

Compared to conventional antennas, the proposed structure offers several advantages. Its compact form factor makes it suitable for space-constrained environments, while its low power consumption supports battery-powered operation for extended periods. The design's reconfigurable nature ensures scalability and adaptability across different use cases—ranging from smart home automation, environmental monitoring, and agricultural sensing, to wearable health devices and industrial IoT (IIoT) platforms[15,16]. By minimizing signal loss, reducing interference, and enhancing spectral efficiency, the antenna design contributes significantly to the realization of reliable and high-performance IoT systems.

The next section reviews literature on frequency reconfigurable antennas and metamaterial designs. Ref.[17] presents a printed star-triangular fractal microstrip-fed monopole antenna with a semi-elliptical ground plane designed for super-wideband (SWB) applications. Unlike traditional SWB and fractal antennas, this one is compact and achieves a VSWR of less than 2 at 2.1, 2.45, 3.2, and 3.5 GHz. Ref.[18] describes an extremely wideband star-star fractal antenna fed by a microstrip line, incorporating a semi-elliptical ground plane with notch loading. This design achieves a bandwidth ratio of 11.31:1 with VSWR values below 2. Ref.[19] discusses a metamaterial and slot-based fractal antenna designed for multiband operation at 3.5, 5.01, 3.2, and 5.77 GHz, featuring an L-shaped slot, a Sierpinski triangle (fractal), and a metamaterial circular split ring resonator (SRR) ground plane. Ref.[20] proposes a simple, frequency-reconfigurable microstrip patch antenna for multiband applications, with a 1.8 mm gap between two patches on the same FR4 substrate. Three RF pin diodes are used to modify the antenna's resonance frequencies, allowing operation at 2.4, 4.26, 4.32, and 4.58 GHz with acceptable return loss. Ref.[21] introduces a novel reconfigurable sub-6 GHz microstrip patch antenna operating at 3.9 and 4.9 GHz, which includes a metamaterial (MTM) array and a corresponding printed circuit around a strip line. Ref.[22] describes a frequency-reconfigurable planar monopole antenna using an FR4 substrate, with operation at 2.4, 3.5, 4.7, and 5.8 GHz and radiation efficiency between 73 and 79%, with a VSWR of less than 1.5. Ref.[23] presents a wireless frequency-reconfigurable antenna with a complementary four-split ring resonator (SRR) metamaterial, operating at 3.02, 2.34, 5.06, 6.44, and 4.2 GHz, making it ideal for IoT applications. A major challenge in antenna design is achieving compact size and extended frequency ranges. This research aims to address these issues by leveraging metamaterials, which possess unique electromagnetic properties that enable smaller antenna designs. The research concludes with Sections III and IV, which detail the simulated analysis of the antenna's performance.

Materials and methods
Design of the metasurface unit cell
Recent advancements in metamaterials have enabled the design of innovative unit cells with exceptional electromagnetic properties. In this study, this work presents a Multi-Path T-Structured Unit Cell with single-negative characteristics, operating at 12.1 GHz. The unit cell is fabricated using an FR-4 substrate (1.4 mm thick) with copper cladding (0.035 mm). At this frequency, it demonstrates a relative permittivity (εr) of -8 and a relative permeability (μr) of 17.3. The design utilizes multi-path T-structured elements to enhance electromagnetic performance. Figure 1 illustrates the proposed unit cell, and Table 1 details its dimensions. Moreover, Table S6 presents a comprehensive comparison with recently published unit cell designs.

Proposed antenna design
Everything from the theory and design of the metamaterial-based RA to its fundamental geometry and switching mechanics is addressed here. In order to make the antenna work in two different frequency bands, lumped element switch was installed. PIN diode are used to rebuild the measurement setup circuit. Improved operating efficiency in the distant field is a direct outcome of using a partial ground plane.

Structural geometry
Figure 2 illustrates an antenna incorporating a set of metamaterial unit cells arranged in a 4 × 3 array, totaling 12 cells. These cells form the radiating patch in the upper section of the antenna, carefully arranged to enhance or
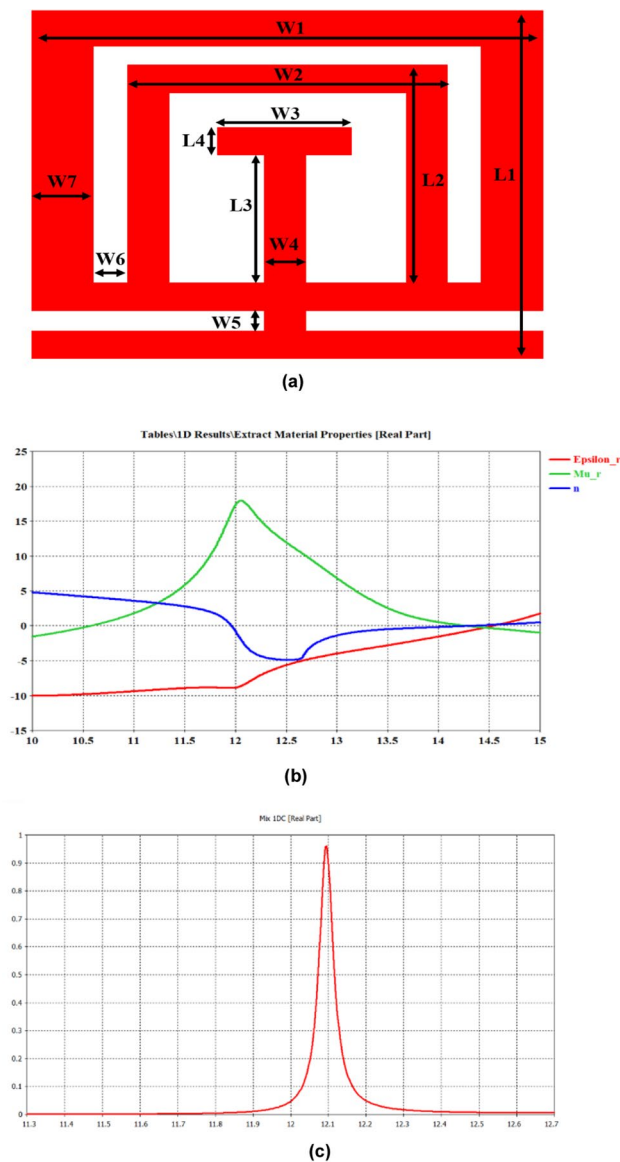
(a)

(b)

(c)

Fig. 1. (**a**) Multi-path T-structured unit cell (**b**) Material properties (**c**) Unit cell absorber.

Parameters	Value (mm)	Parameters	Value (mm)
L1	3.6	W2	2.9
L2	2.29	W3	1.35
L3	1.29	W4	0.5
L4	0.31	W5	0.16
W1	4.78	W6	0.31
W7	0.55		

Table 1. Dimensions of unit cell.

modify performance across specific frequency ranges. The integrated metamaterials consist of small, repetitive elements with intricate patterns. The primary purpose of incorporating these metamaterials is to improve antenna characteristics, such as frequency control and radiation direction. These cells influence the interaction between electromagnetic signals and the material. The inclusion of 12 metamaterial cells enables the antenna to operate at two distinct frequencies, rather than a single frequency. This effect arises from the unique design of the metamaterial cells, which alter the propagation of electromagnetic waves within the antenna structure, The dimensions of the proposed antenna are listed in Table 2.
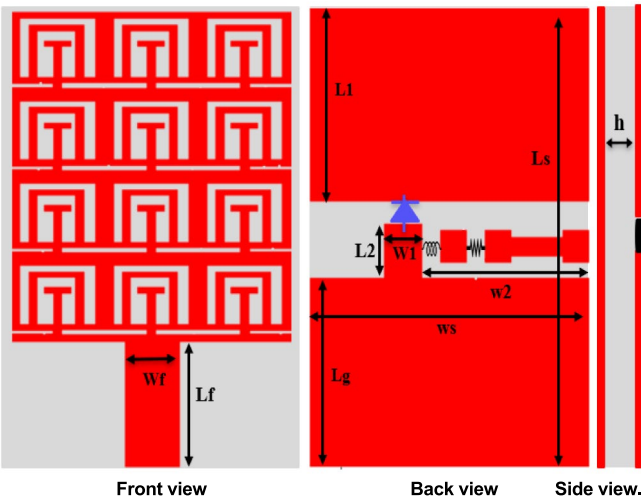
Fig. 2. Geometry of the suggested antenna.

Parameters	Value (mm)	Parameters	Value (mm)
Ls	20	Ws	15
Lg	8.2	Wf	2.745
Lf	5.5	W1	2
L1	8.4	W2	9
L2	2.4	h	1.4

Table 2. Dimensions of the planned antenna.

Theoretically, effective resonant lengths at required frequencies are computed using the transmission line model[24]. For the selected operating frequency f, the effective permittivity εeff and effective resonant length Lf are determined by Eqs. (1) and (2).

$$\varepsilon_{\text{eff}} = \frac{\varepsilon_{\text{r}} + 1}{2} + \frac{\varepsilon_{\text{r}} - 1}{2}\left(1 + 12\left(\frac{h}{w}\right)\right)^{-0.5} \tag{1}$$

$$Lf = \frac{C}{4f\sqrt{\varepsilon_{\text{eff}}}} \tag{2}$$

The variables in the equations are defined as follows: The symbol C denotes the velocity of light in a vacuum, whereas ε_{r} indicates the relative permittivity, h denotes the thickness or height of the substrate, whereas w denotes patch width.

Result and discussion
The proposed design has been analyzed using CST Microwave Studio 2022. The radiating structure is excited through a waveguide port. Performance parameters, including S-parameters, gain, and surface current distributions, can be obtained under various conditions within the CST Microwave Studio environment.

Reconfigurability
Figure 3 illustrates the S-parameter characteristics of the proposed antenna across all operational modes. Mode 1 (D1 OFF), The antenna operates in a single-band mode centered at 2.4 GHz, with a bandwidth of 80 MHz (ranging from 2.36 to 2.44 GHz) and an S-parameter value of − 22.2 dB, indicating efficient impedance matching at this frequency. Mode 2 (D1 ON) The antenna switches to a single-band mode at 6.04 GHz, achieving a bandwidth of 300 MHz (ranging from 5.9 to 6.2 GHz) and an impressive S-parameter value of − 38.79 dB, reflecting excellent performance in this mode (Table 3).

Switching techniques
The SMP1340-079LF PIN diode is widely used in switching applications due to its RF characteristics. It behaves like a variable resistor and operates efficiently from 10 MHz to 10 GHz. Incorporating PIN diodes into antenna systems enables reconfigurability by altering the effective resonant length of the antenna, thereby influencing the operating frequency. Depending on the applied configuration, the PIN diodes can function as either open-circuit or short-circuit elements, with the forward and reverse modes of operation modeled using equivalent
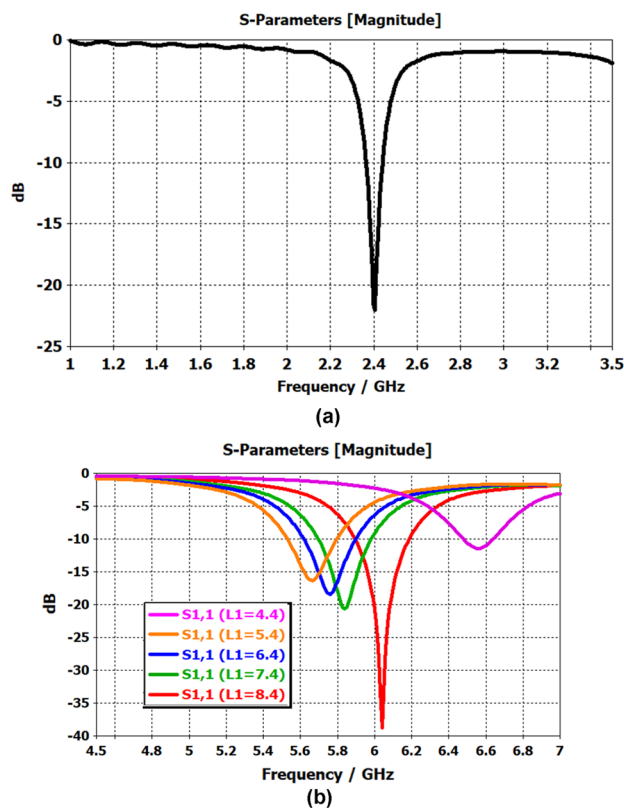
Fig. 3. Mode 2 (**a**) Lg = 8.2, (**b**) L1 = 8.4 mm.

Modes	D1	Frequency band (GHz)	S11 (dB)
1	OFF	2.4	− 22.2
2	ON	6.04	− 38.79

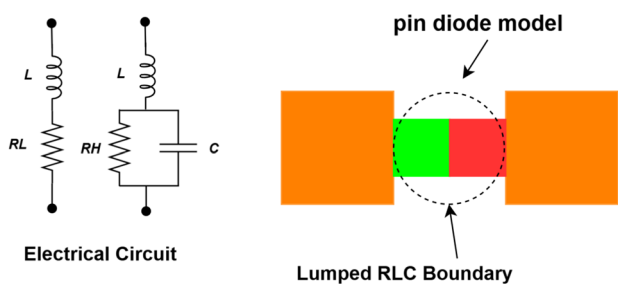**Table 3**. Frequencies and modes of antenna.

Fig. 4. A PIN diode's equivalent circuits and its CST model.

circuits, as illustrated in Fig. 4. For this study, the Skyworks SMP1340-079LF PIN diode was selected, featuring an inductance (L) of 0.7 nH, a series resistance (RL) of 0.85 ohms, and a capacitance (C) of 0.21 pF, making it well-suited for the intended application.

The antenna demonstrates excellent impedance matching, with a voltage standing wave ratio (VSWR) remaining consistently below 1.18 at all resonant bands. This superior performance ensures minimal reflection and efficient power transfer. Figure 5 highlights this capability, showing that the VSWR stays well below the standard threshold of 2 across all usable frequency bands, confirming the antenna's effectiveness in maintaining stable and reliable operation (Fig. 6).
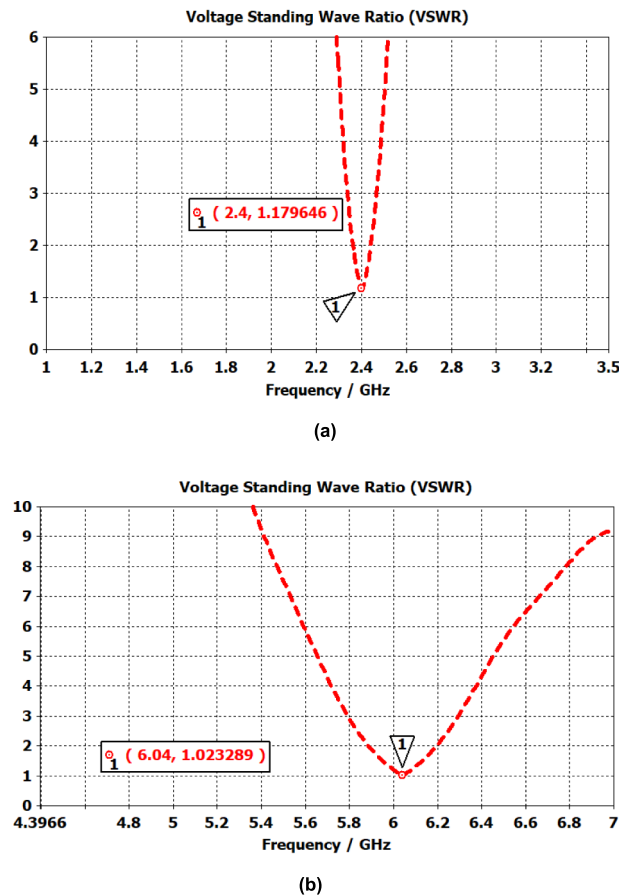
Fig. 5. (a), (b), VSWR of the suggested antenna in various modes of operation.

Biasing circuit

On the same FR-4 substrate, a biasing circuit for the proposed antenna's PIN diode switch was designed and implemented. Figure 7 illustrates the control mechanism, where a bias line connects to a bias pad to activate the PIN diode switch as a proof of concept. The switch is connected to the negative terminal of a 3-V DC battery, while the positive terminal is directly linked to the bias circuit. This setup enables the switch to control the flow of voltage, toggling the diodes ON and OFF. The direct connection of the DC terminal, as shown, makes this design adaptable for future applications, such as cognitive radio systems. To protect the PIN diode, specific design gaps were incorporated: a 1 mm gap between the bias pad and the ground to accommodate inductors (H), and an additional 1 mm gap between two pad lines to place a 1 kΩ resistor (R) for added protection. The DC circuit is isolated from the antenna's feeding line using RF chokes, which block RF signals while permitting DC current flow. Key components include a 1 kΩ resistor to regulate and protect the voltage and 47 nH inductors for additional stability. Figure 6 presents the measurement results of the reconfigurable monopole antenna's reflection coefficient (S11) using an Agilent Technologies E5071C network analyzer (30 kHz–20 GHz) at Al-Nahrain University, Baghdad, Iraq. The antenna operates with a bias current of approximately 2.2 mA (calculated using Ohm's law with a 1 kΩ resistor) and a bias voltage of 3 V, powered by two 1.5-V DURA Cell alkaline batteries.

For the inductors (47 nH), the inductive reactance (X_L) is calculated as:

$$X_L = 2\pi f L \tag{3}$$

where f at 1 GHz:

$$X_L = 2\pi \times 10^9 \times 47 \times 10^{-9} = 295\,\Omega$$

At DC (frequency = 0 Hz), the reactance is 0, and the inductor acts as a short circuit, allowing DC to pass freely. This can be calculated as:

$$X_L = 2\pi \times 0 \times 47 \times 10^{-9} = 0\,\Omega$$

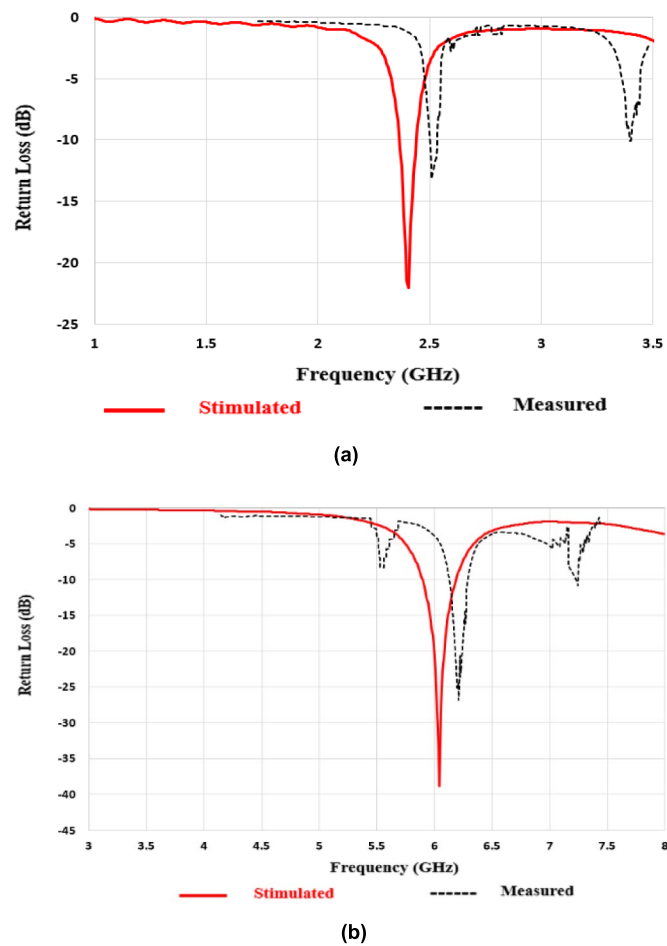To determine the current passing through the PIN diode, we use Ohm's law:

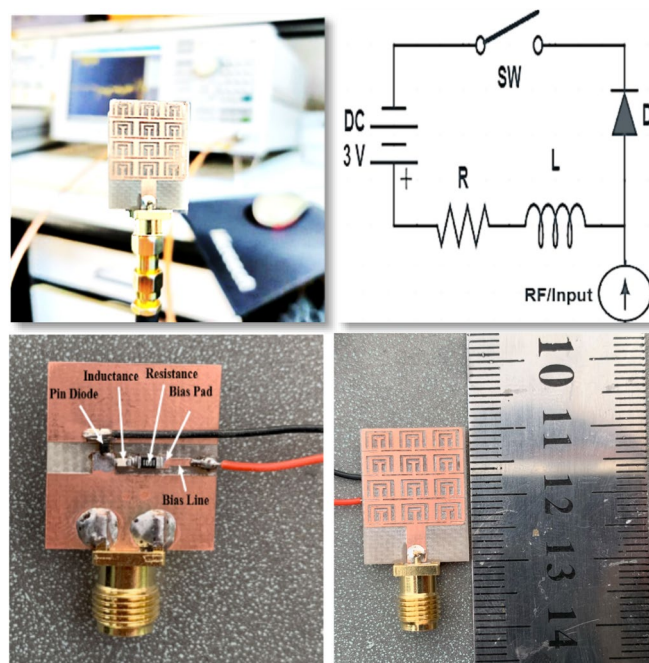Fig. 6. (a), (b), Practical result of the two modes.

Fig. 7. Biasing circuit and antenna proposed.

$$I_R = \frac{V_{cc} - V_{diode}}{R} \tag{4}$$

where $Vcc = 3$ Volts(power supply voltage) and $R = 1\,\text{k}\Omega$. For example:

$$I_R = \frac{3 - 0.8}{1000} = 2.2\,\text{mA}$$

This ensures that the current passing through the PIN diode remains within the safe operating range to ensure its proper functioning.

As for the power consumption in the ON state (D1 ON), the consumed power is calculated using the equation:

$$\text{P} = \text{V} \times \text{I} \tag{5}$$

$$3\,\text{V} \times 2.2\,\text{mA} = 6.6\,\text{mW}$$

This value represents the power consumed when the PIN diode is activated to switch to the higher frequency (6.04 GHz). Regarding the total energy cost, assuming the antenna operates in the ON state (D1 ON) for 50% of the time, the average power consumption would be:

$$\text{P}_{\text{avg}} = \frac{6.6\,\text{mW}}{2} = 3\ \text{mW} \tag{6}$$

This is a very low value, making the antenna highly suitable for battery-powered applications such as Internet of Things (IoT) devices.

Physical interpretation

The operation of the antenna at the frequencies 2.4 and 6.04 GHz depends on the relationship between the antenna's effective length and the electromagnetic properties resulting from its design, including the addition of metamaterials. Resonance in the antenna occurs when its effective length is equal to half the wavelength of the signal at the resonant frequency. The effective length (Leff) is mathematically determined by the following equation[24]:

$$\text{Lf} = \frac{\text{C}}{2\text{f}} \tag{7}$$

The effective length at 2.4 GHz is 62.5 mm and at 6.04 GHz is 24.8 mm.

Metamaterials perform a crucial role in reducing the effective length of an antenna, allowing it to operate at lower frequencies while maintaining smaller physical dimensions. The effective wavelength is modified according to the relationship[24]:

$$\lambda_{\text{eff}} = \frac{\lambda}{\sqrt{\varepsilon_{\text{eff}}\mu_{\text{eff}}}} \tag{8}$$

Metamaterials with negative values, such as ε_{eff}(-8) and μeff (17.3), reduce the effective wavelength, allowing the antenna to resonate at desired frequencies with smaller dimensions. When the switch is OFF, the ground plane is small, causing surface currents to extend more over the radiating patch and along the edges. This increases the effective length, resulting in a lower resonant frequency of 2.4 GHz. Conversely, when the switch is ON, the ground plane area increases. The larger ground plane reduces the spread of surface currents across the antenna. Instead of extending to the edges, the currents are concentrated within a shorter path. This reduction in the effective length leads to a higher resonant frequency of 6.04 GHz.

Far field radiation pattern

In Mode 1, the simulation results show a gain of 3.7 dBi at 2.4 GHz with a radiation efficiency of 95.6%. In Mode 2, the antenna achieved a gain of 4.82 dBi and a radiation efficiency of 92% at 6.04 GHz. Figure 8 presents the simulated radiation patterns of the antenna in both the H-plane and E-plane across the respective frequency bands and Fig. 9 illustrates the gain and radiation intensity for both modes.

Surface currents

Figure 10 illustrates the surface current distribution on the antenna's radiating structure at various frequencies, demonstrating how the distribution changes across different operating modes. At 2.4 GHz, the primary radiating element shows a surface current density that plays a significant role in radiation. As the frequency increases to 6.04 GHz, the surface current distribution undergoes noticeable alterations due to the shorter wavelength. At this higher frequency, the antenna excites higher-order modes, resulting in more complex and rapid variations in the surface currents. These variations create multiple regions of concentrated current density, which influence the radiation pattern and overall performance of the antenna at the higher frequency.

Finally, A comparison between the theoretical and experimental results is presented in Table 4, a summary of the design as shown in Table 5, and a comparison of the proposed antenna to previously published studies in Table 7 (Table 6).
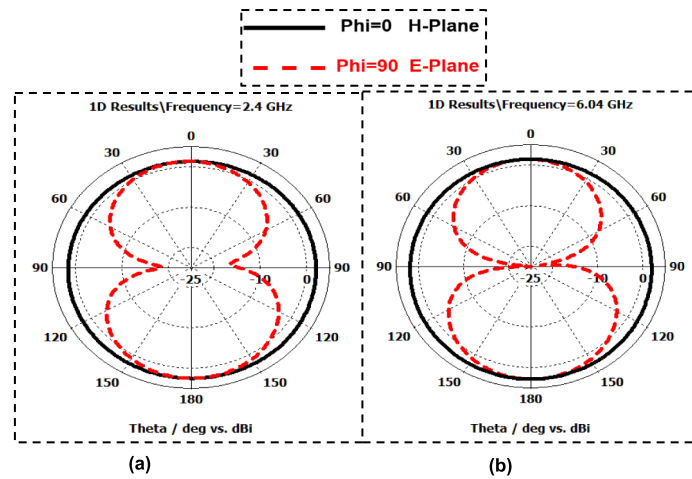
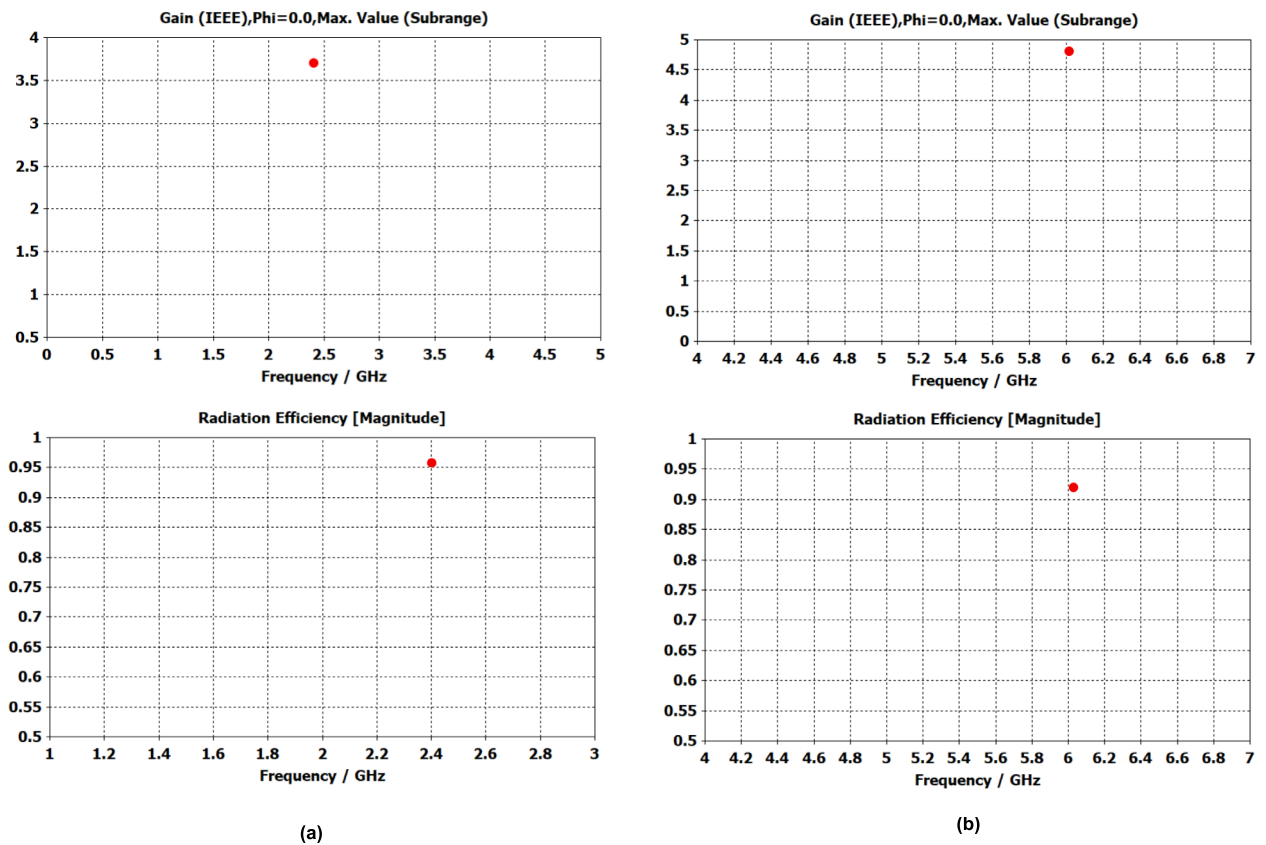**Fig. 8**. The Radiation pattern in the E-plane and H-plane. (**a**) 2.4 GHz, (**b**) 6.04 GHz.

Fig. 9. Gain and efficiency pattern at frequencies (**a**), MODE 1(2.4 GHz), (**b**) MODE 2 (6.04 GHz).

Conclusion and future work

There is increasing interest in designing compact antennas without compromising performance, particularly at lower frequencies crucial for IoT applications. The proposed antenna, with dimensions of $20 \times 15 \times 1.4$ mm^3, operates at 2.4 GHz and 6.04 GHz, achieving reconfigurability through strategically placed PIN diodes while maintaining a reflection coefficient below − 10 dB. This compact design addresses the need for efficient, space-saving antennas in IoT systems. Despite the good agreement between simulation results and theoretical predictions, minor discrepancies were observed. These variations can be attributed to manufacturing inaccuracies, slight misalignments of components, and environmental variations such as temperature or humidity changes during testing. Addressing these challenges through improved fabrication techniques and
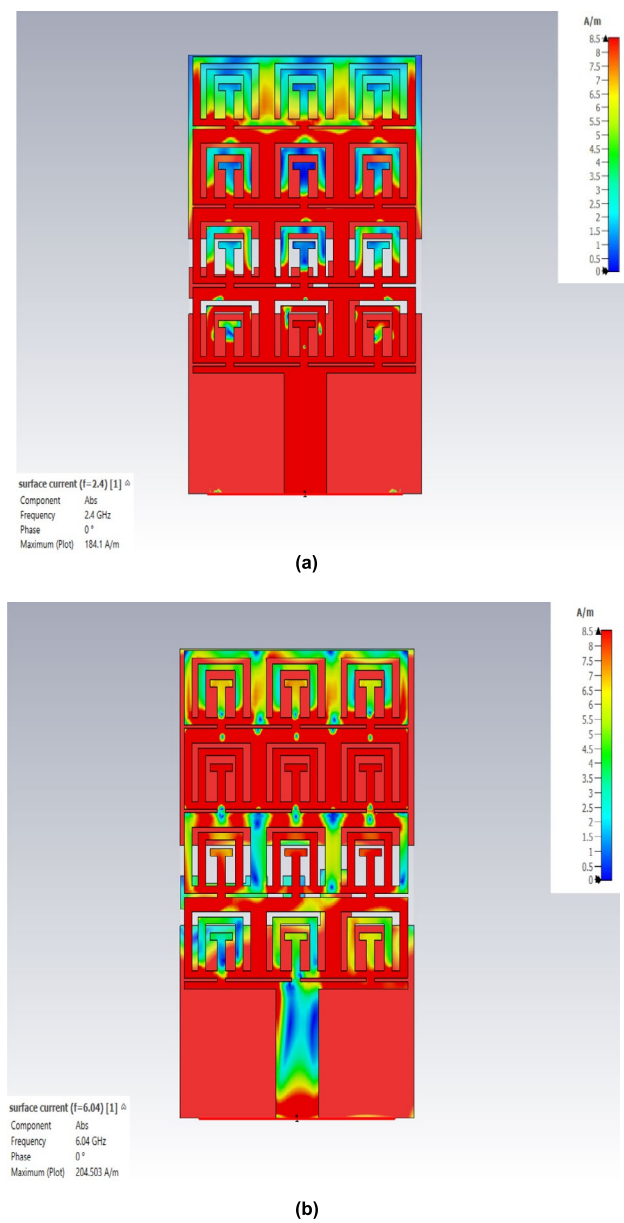
(a)

(b)

Fig. 10. Distribution of current (**a**) at 2.4 GHz (**b**) at 6.04 GHz.

Parameters	Simulated	Theoretical	Observed Deviations
Frequencies (2.4 GHz)	2.4 GHz	2.5 GHz	4.17% shift
Frequencies (6.04 GHz)	6.04 GHz	6.23 GHz	3.15% shift
S11 (2.4 GHz) dB	− 22.2 dB	− 13	9.2 dB (weaker matching)
S11 (6.04 GHz) dB	− 38.79	− 27.3	11.49 dB (weaker matching)
Bandwidth (2.4 GHz) MHz	80	59	26.25%
Bandwidth (6.04 GHz) MHz	300	214	28.7%

Table 4. Comparison between simulated and experimental results.

controlled testing conditions could further enhance performance consistency. The integration of metamaterials into antenna design enhances performance for a wide range of applications, including communications and remote sensing. For IoT, the antenna demonstrates high efficiency and adaptability in constrained spaces. Future advancements, such as expanding frequency ranges and integrating AI technologies, could enable autonomous operation, minimize electromagnetic interference, and further miniaturize the design to suit wearable devices

Parameters	Antenna
Substrate	FR-4
Dimensions (mm)	$20 \times 15 \times 1.4$
Operating frequencies (GHz)	(2.4, 6.02) GHz
bandwidth	(0.08–0.3) GHz
No of operating bands	2
Biasing complexity	Bias circuits combine the same antenna
Gain (dBi)	3.7–4.82
VSWR	Less than 1.18
Efficiency%	92–95.6
Switch	Real switch
Feeding method	Microstrip Line
Metamaterial inclusion	4*3-unit cell
Design type	Practical

Table 5. Summary of the design.

References	Resonator type	Unit Cell size (mm)	Absorption frequency (GHz)	Absorption (%)	Applications
[25]	Ring	12×12	9.828	99.99	EMI shielding
[26]	Octagonal Close Ring	8×8	6.45, 14.89	99.15, 99.76	Satellite
[27]	Circular Sector	10×10	6.68, 15.41	Over 99	Microwave
[28]	Gap Coupled Hexagonal	10×10	4.27, 5.42, 12.40	99, 98, 81	Microwave
[29]	Square with Circular Ring	10×10	5.35, 7.29, 11.85	82, 67, 93	Microwave
[30]	Four Quarters of Circle	9×9	9.12, 11.34	99.35, 97.81	Microwave
[31]	Double E-shaped	10×10	5.376, 10.32, 12.25	99.9, 99.9, 99.7	EMI shielding
This work	Multi-Path T-shape	3.6×4.78	12.1	96	Microwave

Table 6. Comparison of the proposed work with recently published metamaterial.

References	Antenna size $mm^3/(\lambda_o^3)$	Reconfiguration type	Frequency bands (GHz)	Antenna type	No. of switches	Max Gain (dBi)
[32]	$25 \times 25 \times 1.6$ $(0.32 \times 0.32 \times 0.02)$	Frequency	3.85/4.14/4.43/4.91/6.01	Rectangular slotted with defected ground	3 PIN diodes	4.42
[33]	$40 \times 50 \times 0.254$ $(0.22 \times 0.27 \times 0.001)$	Frequency and radiation pattern	(1.65–2.5)/1.8/2.1	Triangular monopole	2 PIN diodes	2.2
[34]	$20 \times 20 \times 0.8$ $(0.21 \times 0.21 \times 0.008)$	Frequency	3.22/4.99/7.35/7.26	Slot-based square-shaped monopole	1 PIN diode	3.8
[35]	$40 \times 40 \times 1.5$ $(0.18 \times 0.18 \times 0.007)$	Frequency	Continuous tuning (1.4–2.9)	Hexagonal patch element	1 Varactor diode	2.4
[36]	$32 \times 25 \times 0.254$ $(0.19 \times 0.15 \times 0.001)$	Frequency	1.8/1.9/2.1/2.45/3.5	Quarter-wave monopole with filtering stub	3 PIN diodes	3.2
[37]	$35 \times 25 \times 0.254$ $(0.28\lambda_o \times 0.20\lambda_o \times 0.002\lambda_o)$	Frequency	(2.76–8.21)/2.45/5.8/5.2/8	CPW-fed slotted circular patch	1 PIN diode	5.8
[38]	$30 \times 30 \times 0.13$ $(0.24 \times 0.24 \times 0.001)$	Frequency	2.4/3.5/4	CPW-fed monopole	2 PIN diodes	2.95
[38]	$77 \times 77 \times 15$ $(0.61 \times 0.61 \times 0.21)$	Frequency	2.4/3.5/4	CPW-fed monopole	2 PIN diodes	7.9
[39]	$28 \times 14 \times 1$ $(0.228 \times 0.114 \times 0.008)$	Frequency	(5.6–4.6)/3.5/2.45	Wave-guide monopole	2 PIN diodes	4
[40]	$30 \times 30 \times 1.6$ $(0.41 \times 0.41 \times 0.021)$	Frequency	5.2/4.1	Wave-guide monopole	1 PIN diodes	4
[23]	$38 \times 21 \times 1.6$ $(0.23 \times 0.127 \times 0.0097)$	Frequency	3.02, 2.34, 5.06, 1.82, 4.2, 6.44	Wave-guide monopole	2 PIN diodes	2.56
This work	$20 \times 15 \times 1.4$ $(0.16 \times 0.12 \times 0.0112)$	Frequency	6.04/2.4	Wave-guide monopole	1 PIN diodes	4.82

Table 7. Proposed antenna is contrasted with previously published research.

and embedded systems. Future work will focus on improving manufacturing precision, addressing environmental challenges, and exploring new applications in healthcare, environmental monitoring, and industrial automation, these improvements will enable innovative solutions for wireless communication and IoT systems.

Data availability
Data is provided within the manuscript.

References
1. Islam, M. S. et al. A modified meander line microstrip patch antenna with enhanced bandwidth for 2.4 GHz ISM-band Internet of Things (IoT) applications. *IEEE Access* **7**, 127850–127861 (2019).
2. Azim, R., Islam, M. T. & Mobashsher, A. T. Design of a dual band-notch UWB slot antenna by means of simple parasitic slits. *IEEE Antennas Wirel. Propag. Lett.* **12**, 1412–1415 (2013).
3. Abd, A. K. & Rasool, J. M. Octa-band reconfigurable monopole antenna frequency diversity 5G wireless. *Int. J. Electr. Comput. Eng.* **13**(2), 1606–1617 (2023).
4. Colaco, J. & Lohani, R. Design and implementation of microstrip circular patch antenna for 5G applications. In *2020 International Conference on Electrical, Communication, and Computer Engineering (ICECCE)* 1–4. (IEEE, 2020).
5. Sharma, B. L., Mathur, D. & Sharma, M. K. SIW-cavity based frequency reconfigurable antenna for IoT, WLAN, and 5G applications. *Frequenz* **77**(7–8), 413–424 (2023).
6. Abdulhussein, A. J., Farhan, M. J. & Ali, G. M. Design and implementation of a frequency reconfigurable antenna using PIN switch for sub-6 GHz applications. *Open Eng.* **13**(1), 20220453 (2023).
7. Abd, A. K. & Rasool, J. M. Low-profile frequency-reconfigurable antenna for 5G applications. *TELKOMNIKA (Telecommun. Comput. Electron. Control)* **21**(3), 486–495 (2023).
8. Abd, A. K., Rasool, J. M., Rahman, Z.-A.S. & Al-Yasir, Y. I. Design and analysis of novel reconfigurable monopole antenna using DIP switch and covering 5G-sub-6-GHz and C-band applications. *Electronics* **11**(20), 3368 (2022).
9. Abd, A. K. & Rasool, J. M. A frequency reconfigurable monopole antenna diversity for 5G wireless communication and IoT applications. In *2022 8th International Conference on Contemporary Information Technology and Mathematics (ICCITM)* 243–248. (IEEE, 2022).
10. Rahman, A., Islam, M. T., Singh, M. J., Kibria, S. & Akhtaruzzaman, M. Electromagnetic performances analysis of an ultra-wideband and flexible material antenna in microwave breast imaging: To implement a wearable medical bra. *Sci. Rep.* **6**(1), 38906 (2016).
11. Saeed, S. M., Balanis, C. A., Birtcher, C. R., Durgun, A. C. & Shaman, H. N. Wearable flexible reconfigurable antenna integrated with artificial magnetic conductor. *IEEE Antennas Wirel. Propag. Lett.* **16**, 2396–2399 (2017).
12. Nasir, U. et al. A compact frequency reconfigurable CPS-like metamaterial-inspired antenna. *Microw. Opt. Technol. Lett.* **59**(3), 596–601 (2017).
13. Islam, M. T., Cho, M., Samsuzzaman, M. & Kibria, S. Compact antenna for small satellite applications [Antenna Applications Corner]. *IEEE Antennas Propag. Mag.* **57**(2), 30–36 (2015).
14. Hussain, M. et al. Metamaterials and their application in the performance enhancement of reconfigurable antennas: A review. *Micromachines* **14**(2), 349 (2023).
15. Almutairi, A. F. et al. A complementary split ring resonator based metamaterial with effective medium ratio for C-band microwave applications. *Results Phys.* **15**, 102675 (2019).
16. Misran, N., Yusop, S. H., Islam, M. T. & Ismail, M. Y. Analysis of parameterization substrate thickness and permittivity for concentric split ring square reflectarray element. *Jurnal Kejuruteraan* **23**, 11–15 (2011).
17. Waladi, V., Mohammadi, N., Zehforoosh, Y., Habashi, A. & Nourinia, J. A novel modified star-triangular fractal (MSTF) monopole antenna for super-wideband applications. *IEEE Antennas Wirel. Propag. Lett.* **12**, 651–654 (2013).
18. Singhal, S. & Singh, A. K. Modified star-star fractal (MSSF) super-wideband antenna. *Microw. Opt. Technol. Lett.* **59**(3), 624–630 (2017).
19. Ali, T., Aw, M. S. & Biradar, R. C. A fractal quad-band antenna loaded with L-shaped slot and metamaterial for wireless applications. *Int. J. Microw. Wirel. Technol.* **10**(7), 826–834 (2018).
20. Saikia, B., Dutta, P. & Borah, K. Design of a frequency reconfigurable microstrip patch antenna for multiband applications. In *Proceedings of the 5th International Conference on Computers & Management Skills (ICCM 2019)| North Eastern Regional Institute of Science & Technology (NERIST), Nirjuli, Arunachal Pradesh, India* (2020).
21. Al-Khaylani, H. H., Elwi, T. A. & Ibrahim, A. A. A novel miniaturized reconfigurable microstrip antenna based printed metamaterial circuitries for 5G applications. *Prog. Electromagn. Res* **120**, 1–10 (2022).
22. Thenkumari, K., Sankaran, K. S. & Mathana, J. Design and implementation of frequency reconfigurable antenna for Wi-Fi applications. *Eng. Sci.* **23**(2), 876 (2023).
23. Rasool, J. M. & Abd, A. K. A reconfigurable antenna for IOT applications with enhanced performance by adding metamaterial. *J. Commun.* **19**(4), 198–203 (2024).
24. Balanis, C. A. *Antenna Theory: Analysis and Design* (Wiley, 2016).
25. Mishra, R. K., Gupta, R. D. & Datar, S. Metamaterial microwave absorber (MMA) for electromagnetic interference (EMI) shielding in X-band. *Plasmonics* **16**(6), 2061–2071 (2021).
26. Afsar, M. S. U. et al. A new octagonal close ring resonator based dumbbell-shaped tuning fork perfect metamaterial absorber for C-and Ku-band applications. *Micromachines* **13**(2), 162 (2022).
27. Nguyen, T. Q. H., Nguyen, T. K. T., Cao, T. N., Nguyen, H. & Bach, L. G. Numerical study of a broadband metamaterial absorber using a single split circle ring and lumped resistors for X-band applications. *AIP Adv.* **10**(3), 64 (2020).
28. Zhang, Y. et al. High-performance broadband electromagnetic interference shielding optical window based on a metamaterial absorber. *Opt. Express* **28**(18), 26836–26849 (2020).
29. Islam, M. S. et al. A gap coupled hexagonal split ring resonator based metamaterial for S-band and X-band microwave applications. *IEEE Access* **8**, 68239–68253 (2020).
30. Ashraf, F. B., Alam, T., Kibria, S. & Islam, M. T. A compact meander line elliptic split ring resonator based metamaterial for electromagnetic shielding. *Mater. Express* **8**(2), 133–140 (2018).
31. Hossain, M. B., Faruque, M. R. I., Islam, M. T., Singh, M. & Jusoh, M. Triple band microwave metamaterial absorber based on double E-shaped symmetric split ring resonators for EMI shielding and stealth applications. *J. Market. Res.* **18**, 1653–1668 (2022).
32. Singh, P. P., Goswami, P. K., Sharma, S. K. & Goswami, G. Frequency reconfigurable multiband antenna for IoT applications in WLAN, Wi-Max, and C-band. *Progress Electromag. Res. C* **102**, 149–162 (2020).
33. Ghaffar, A. et al. A flexible and pattern reconfigurable antenna with small dimensions and simple layout for wireless communication systems operating over 1.65–2.51 GHz. *Electronics* **10**(5), 601 (2021).

34. Sanjeeva Reddy, B., Darimireddy, N. K., Park, C.-W. & Chehri, A. Performance of reconfigurable antenna fabricated on flexible and nonflexible materials for band switching applications. *Energies* **14**(9), 2553 (2021).
35. Riaz, S., Khan, M., Javed, U. & Zhao, X. A miniaturized frequency reconfigurable patch antenna for IoT applications. *Wirel. Person. Commun.* **8**, 1–11 (2022).
36. Awan, W. A., Hussain, N., Kim, S. & Kim, N. A frequency-reconfigurable filtenna for GSM, 4G-LTE, ISM, and 5G Sub-6 GHz band applications. *Sensors* **22**(15), 5558 (2022).
37. Hussain, N. et al. A conformal frequency reconfigurable antenna with multiband and wideband characteristics. *Sensors* **22**(7), 2601 (2022).
38. Ibrahim, A. A., Mohamed, H. A., Abdelghany, M. A. & Tammam, E. Flexible and frequency reconfigurable CPW-fed monopole antenna with frequency selective surface for IoT applications. *Sci. Rep.* **13**(1), 8409 (2023).
39. Elwi, T. A., Al-Shaikhli, A. A., Al-Khaylani, H. H. & Abdulsattar, R. K. Reconfigurable metamaterial antenna based an electromagnetic ground plane defects for modern wireless communication devices. *Adv. Electromag.* **13**(1), 39–43 (2024).
40. Karthiga, B. & Mahendran, C. A compact dual-band frequency reconfigurable antenna with pin diode integration for smartwatch application. *Int. J. Electron. Lett.* **12**(4), 403–412 (2024).

Acknowledgements

Author contributions

A.H.A.: Conceptualization, methodology, investigation, validation, writing—original draft. J.M.R.: Supervision, project administration, software. M. S. I.: Investigation, writing-review & editing, validation. M.T.I.: Administration, resources, Supervision, Visualization, data curation, M.A.A.: Validation, writing-review & editing. A.K.A.: Investigation, writing-review & editing. M.O.: Visualization, data curation, validation. M.A.A.: Visualization, data curation, validation.

Funding

Declarations

Competing interests

The authors declare no competing interests.

Additional information

Correspondence and requests for materials should be addressed to A.H.A., M.S.I. or M.T.I.

Reprints and permissions information is available at www.nature.com/reprints.

Publisher's note Springer Nature remains neutral with regard to jurisdictional claims in published maps and institutional affiliations.